Coastal Education & Research Foundation, Inc.

Determining the Damage Mechanisms for Buoyancy Materials of Deep-Sea Manned Submersibles

Author(s): Yi Zhang, Zhongjun Ding, Yifan Wang, Qingxin Zhao and Shengjie Qin
Source: *Journal of Coastal Research*, Vol. 35, No. 5 (September 2019), pp. 996-1002
Published by: Coastal Education & Research Foundation, Inc.
Stable URL: https://www.jstor.org/stable/26778548
Accessed: 17-05-2021 09:13 UTC

REFERENCES
Linked references are available on JSTOR for this article:
https://www.jstor.org/stable/26778548?seq=1&cid=pdf-reference#references_tab_contents
You may need to log in to JSTOR to access the linked references.

JSTOR is a not-for-profit service that helps scholars, researchers, and students discover, use, and build upon a wide range of content in a trusted digital archive. We use information technology and tools to increase productivity and facilitate new forms of scholarship. For more information about JSTOR, please contact support@jstor.org.

Your use of the JSTOR archive indicates your acceptance of the Terms & Conditions of Use, available at https://about.jstor.org/terms

Coastal Education & Research Foundation, Inc. is collaborating with JSTOR to digitize, preserve and extend access to *Journal of Coastal Research*

This content downloaded from 159.226.142.168 on Mon, 17 May 2021 09:13:52 UTC
All use subject to https://about.jstor.org/terms

Journal of Coastal Research	35	5	996–1002	Coconut Creek, Florida	September 2019

Determining the Damage Mechanisms for Buoyancy Materials of Deep-Sea Manned Submersibles

Yi Zhang[†‡], Zhongjun Ding[‡], Yifan Wang[§], Qingxin Zhao[‡††]*, and Shengjie Qin[‡]

[†]College of Shipbuilding Engineering
Harbin Engineering University
Harbin 150001, China

[‡]National Deep-Sea Center
Qingdao 266061, China

[§]Pilot National Laboratory
for Marine Science and Technology
Qingdao 266237, China

[††]College of Environmental Science
and Engineering
Ocean University of China
Qingdao 266100, China

www.cerf-jcr.org

www.JCRonline.org

ABSTRACT

Zhang, Y.; Ding, Z.; Wang, Y.; Zhao, Q., and Qin, S., 2019. Determining the damage mechanisms for buoyancy materials of deep-sea manned submersibles. *Journal of Coastal Research,* 35(5), 996–1002. Coconut Creek (Florida), ISSN 0749-0208.

Deep-sea manned submersibles are important platforms for ocean exploration, and their structural reliability is critical to the personal safety of the crew. In particular, the buoyancy materials of deep-sea manned submersibles are vital parts because they provide the necessary buoyancy for submersible operations. This paper first describes the overall damage of the buoyancy materials used in the deep-sea manned submersible Jiaolong that accumulated over a large number of research expeditions during years of services. The causes of the damage are analyzed by computational fluid dynamics (CFD) methods. Because Jiaolong's buoyancy materials are secured to its structural frame by bolts, the external forces that act on the submersible are concentrated on these bolts. Those external forces include the wave forces that act on the submersible when it floats on the sea surface and the buoyancy material shrinkage that occurs because of changes in environmental pressure and temperature during submarine operations. Finally, several suggestions are provided for improving the design and operation of deep-sea submersibles.

ADDITIONAL INDEX WORDS: *Wave action, CFD, environmental pressure*.

INTRODUCTION

Manned submersibles are important platforms for ocean exploration and research, and their structural reliability is critical to the personal safety of crew and national scientific properties. In particular, the buoyancy materials are vital structural parts of manned submersibles because they supply the necessary buoyancy for submersible operation. Hence, they should be designed to be durable and should be systematically examined during maintenance (Cui, 2013; Du, Hu, and Cui, 2017; Kohnen, 2013; Stechler and Poneros, 1968).

Research on buoyancy materials began in the 1960s for exploring the deep ocean near seabed. During that time, research mainly focused on the fabrication of buoyancy materials with great strength and low weight. Some of the products included chemical foam buoyancy materials formed by the chemical foaming and solidification of mixed raw materials (Zhang *et al*., 2012); composite syntactic foams formed by the addition of low-density fillers such as ceramic microspheres, large-diameter glass spheres, or metal spheres to syntactic foam buoyancy materials (John and Nair, 2010; Pasco-Anderson and Watkins, 1985; Walden, Tessier, and Popenoe, 2010); and composite materials formed by the heat-curing molding of resin matrices filled with glass microspheres (Cui, Guo, and Pan, 2018; Sun *et al*., 2013). Although numerous researchers have studied the intrinsic properties of buoyancy materials (Gall *et al*., 2014; Jahsman, 1968; Johnson *et al*., 1970; Li, Zhu, and Chen, 2016; Ren *et al*., 2017; Zhang, Wang, and Silberschmidt, 2017), these studies have usually focused on the effect of deep-sea hydrostatic pressures on the buoyancy materials. Very few researchers have investigated the damage caused by external loads on the buoyancy materials in real marine environments.

The selection of buoyancy material is a crucial aspect of designing deep-sea (depth rating: $\geq$7000 m) manned submersibles because the suitability of the buoyancy material directly affects the reliability and safety of the submersible. The buoyancy material must be capable of withstanding high pressures while having low densities, low water absorption rates, and low volumetric shrinkage, as well as excellent machining properties. The properties of the buoyancy material used in Jiaolong are listed in Table 1. The Jiaolong manned submersible successfully dived to 7062 m in the Mariana Trench in 2012. It is the greatest depth achieved in the world by the same type of manned submersible. The buoyancy materials used in the deep-sea manned submersible Jiaolong are made of an epoxy matrix that is filled uniformly with hollow glass microspheres. The material has been very stable throughout the sea trials and experimental expeditions of the submersible over the years. During the 35th Chinese Ocean Expedition, the Jiaolong floated on the sea surface for more than 10 hours under severe sea conditions. During the 37th Chinese Ocean Expedition, the Jiaolong made a series of continuous deep

DOI: 10.2112/JCOASTRES-D-19-00007.1 received 15 January 2019; accepted in revision 21 March 2019; corrected proofs received 22 April 2019; published pre-print online 13 May 2019.
*Corresponding author: zhaoqingxin@ndsc.org.cn
©Coastal Education and Research Foundation, Inc. 2019

This content downloaded from 159.226.142.168 on Mon, 17 May 2021 09:13:52 UTC
All use subject to https://about.jstor.org/terms

Table 1. *Primary technical properties of Jiaolong's buoyancy materials.*

Parameter	Value
Density	0.56×10^3 kg m^{-3}
Compressive strength	68.16 MPa
Shear strength	14.8 MPa
Tensile Strength	26.8 MPa
Bulk modulus	3.73 GPa
Impact toughness	10.1 J m^{-1}
Poisson's ratio	0.3
Water absorption rate (71 MPa, 4 h)	<1%

dives, nine of which achieved a depth of more than 6000 m. Under the influence of severe sea conditions and high-intensity work, the buoyant materials of the submersible began to crack, and this problem recurred in the following expeditions even after maintenance.

The analysis in this study shows that the damage to Jiaolong's buoyancy materials usually manifested in three forms: shear damage, tension-compression damage, and loosening of pre-embedded parts (Figure 1). The shear damage refers to the cracks that propagate in the buoyancy materials; this form of damage usually appears in the four buoyancy material blocks located around the stern stabilizing fins, and the damage is not related to the position of connection holes. Tension-compression damage refers to cracks that appear near the connection holes, and its propagating direction is orthogonal to the line between the two connection holes; this form of damage usually occurs in the larger external buoyancy blocks. The buoyancy materials are not directly attached to the structural frame but are instead attached to preinstalled connection devices called pre-embedded parts. The third form of damage involves the loosening of these parts from the buoyancy blocks because of external forces. The number of instances of each form of buoyancy material damage in the aftermath of the 35th and 37th China Ocean Expeditions are shown in Figure 2. Shear damage was the most common form of damage after the 35th expedition; however, after the 37th expedition, the instances of tension-compression damage and the loosening of pre-embedded parts greatly exceeded the instances of shear damage. On further analysis, it was found that these results are related to the operational environments. As discussed, during the 35th expedition, the submersible floated on the sea surface during extreme sea conditions for an extended period of time. In contrast, the 37th expedition involved long periods of diving operation at great depths. These differences in operational environment led to the differences in the predominant form of damage.

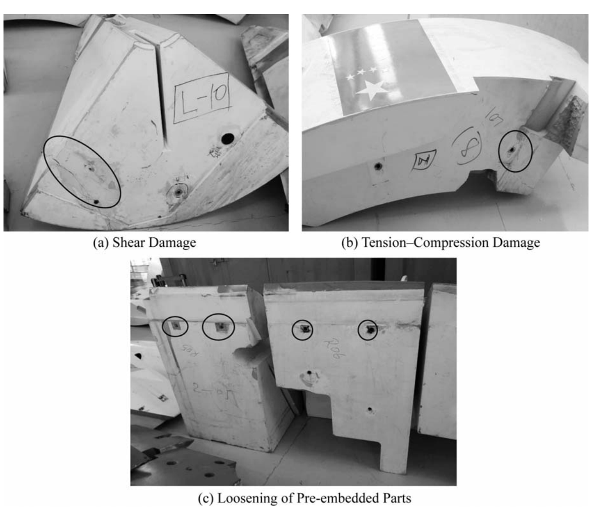

Figure 1. Forms of buoyancy material damage: (a) shear, (b) tension-compression, (c) loosening of pre-embedded parts.

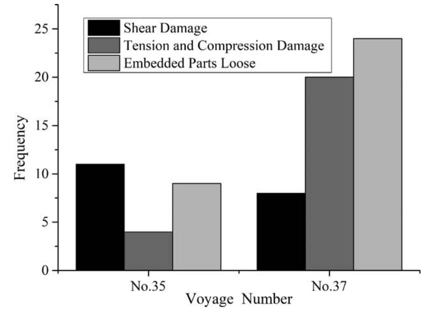

Figure 2. Number of instances of each form of buoyancy material damage.

To analyze the mechanisms of damage in Jiaolong's buoyancy materials, it is necessary first to determine the loads acting on the submersible in its operational environment. The marine operations of Jiaolong can be divided into the following processes: presubmergence preparation, submersible power supply inspections, submersible deployment, surface inspections, submersible submergence, submersible submarine operations, submersible resurfacing, submersible retrieval, and submersible maintenance. The submersible's buoyancy blocks are considerably affected by the following processes: surface inspections, submersible deployment, submersible submergence, submersible submarine operations, submersible resurfacing, and submersible retrieval. The submersible is subjected to wave loads during surface inspections and submersible retrieval, which subsequently affects its structural and buoyancy materials. The most important factor in all other operational stages is water pressure.

METHODS

On the sea surface, the submersible is subjected to wave forces. Because of the outer profile of Jiaolong (Figure 3), most of Jiaolong's components are streamlined and unlikely to be damaged by waves, except for the stern stabilizer fins. Therefore, only the stern stabilizer fins were considered, to simplify the numerical model. The simplified computational fluid dynamics (CFD) model is shown in Figure 4.

The numerical simulations performed in the present work are based on the Reynolds-averaged Navier-Stokes equations:

$$\rho \frac{\partial u_i}{\partial x_i} = 0 \tag{1}$$

$$\rho \frac{\partial}{\partial x_j}\left(u_i u_j\right) = -\frac{\partial p}{\partial x_i} + \rho \frac{\partial}{\partial x_j}\left[v\left(\frac{\partial u_i}{\partial x_j} + \frac{\partial u_j}{\partial x_i}\right)\right] - \frac{\partial}{\partial x_j}\left(-\rho \overline{u_i' u_j'}\right) \tag{2}$$

This content downloaded from 159.226.142.168 on Mon, 17 May 2021 09:13:52 UTC
All use subject to https://about.jstor.org/terms

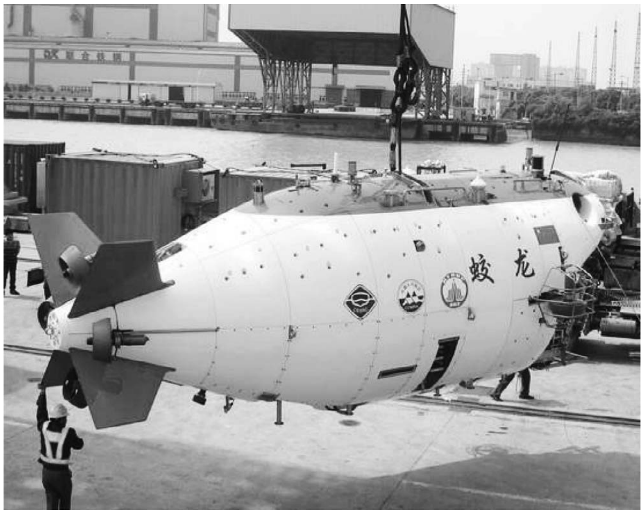

Figure 3. Jiaolong deep-sea manned submersible.

where, u_i and u_j $(i, j = 1, 2, 3)$ are the time-averaged velocity and x_i and x_j $(i,\ j = 1,\ 2,\ 3)$ are the vertical components in the longitudinal, transverse, and vertical directions, respectively; ρ is the density of fluid; p is the time-averaged pressure, v is the kinetic viscosity of water, and $-\rho\overline{u_i'u_j'}$ is the Reynolds stress term.

The shear stress transport (SST) k-ω model requires the solution of transport equations for k and ω:

$$\overrightarrow{U} \cdot \overrightarrow{\nabla} k = v_t S^2 + \overrightarrow{\nabla}\left[\left(v + \frac{v_t}{\sigma_k}\right)\overrightarrow{\nabla} k\right] - \beta^* \omega k \tag{3}$$

$$\overrightarrow{U} \cdot \overrightarrow{\nabla} \omega = \alpha S^2 + \overrightarrow{\nabla}\left[\left(v + \frac{v_t}{\sigma_\omega}\right)\overrightarrow{\nabla} \omega\right] - \beta\omega^2 + F_\omega \frac{1}{\omega}\overrightarrow{\nabla} k \overrightarrow{\nabla} \omega \tag{4}$$

where, S is the mean strain rate.

Eddy viscosity v_t is calculated from:

$$v_t = \frac{a_1 k}{\max(a_1\omega,\ F_2\Omega)} \tag{5}$$

where, $a_1 = 0.31$, and:

$$F_2 = \tanh(\arg_2^2) \tag{6}$$

$$\arg_2 = \max\left(2\frac{\sqrt{k}}{0.09\omega d}, \frac{500v}{\omega d^2}\right) \tag{7}$$

where, Ω is the vorticity magnitude and d is the distance to the wall. The model constants depend on a blending function:

$$F_1 = \tanh\left(\arg_1^4\right) \tag{8}$$

with:

$$\arg = \min\left[\max\left(\frac{\sqrt{k}}{0.09\omega d}, \frac{500v}{d^2\omega}\right), \frac{4\rho(\sigma_\omega)_2 k}{\mathrm{CD}_{kw} d^2}\right] \tag{9}$$

and

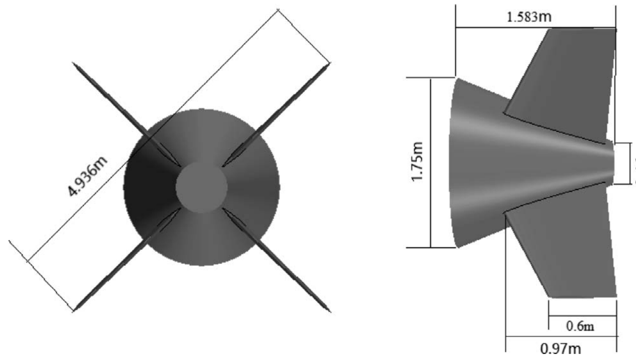

Figure 4. Simplified computational fluid dynamics (CFD) model.

$$\mathrm{CD}_{kw} = \max\left[2\frac{\rho(\sigma_\omega)_2}{\omega}\overrightarrow{\nabla} k \overrightarrow{\nabla} \omega, 10^{-20}\right] \tag{10}$$

where, $\alpha = F_1\alpha_1 + (1 - F_1)\alpha_2$, $\beta = F_1\beta_1 + (1 - F_1)\beta_2$, $\sigma_k = F_1(\sigma_k)_1 + (1 - F_1)(\sigma_k)_2$, $\sigma_\omega = F_1(\sigma_\omega)_1 + (1 - F_1)(\sigma_\omega)_2$, $\alpha_1 = 0.5532$, $\alpha_2 = 0.4404$, $\beta_1 = 0.075$, $\beta_2 = 0.0828$, $(\sigma_k)_1 = 1/0.85$, $(\sigma_k)_2 = 1$, $(\sigma_\omega)_1 = 2$, and $(\sigma_\omega)_2 = 1.17$.

The CFD computations were performed by STAR-CCM+ software, and the waves were simulated with the fifth-order volume-of-fluid waves. This wave more closely resembles a real wave than a wave generated by the first-order method. The wave profile and the wave phase velocity depend on the water depth, wave height, and current. Detailed parameters can be found in the literature (Fenton, 1985). Initially, the central-vertical position of the stabilizer fins was located at the waterline. The left and right walls were defined as symmetrical boundaries, and the inflow inlet was defined as the velocity inlet. The remaining faces were defined as pressure outlets. A numerical wave beach was established at the inlet, outlet, and side boundaries of the tank to avoid reflection. Waves can be damped by introducing resistance to vertical motion. The method devised by (Choi and Yoon, 2009) adds a resistance term to the equation for vertical velocity component w:

$$S_z^d = \rho(f_1 + f_2|w|)\frac{e^\kappa - 1}{e^1 - 1}w \tag{11}$$

with

$$\kappa = \left(\frac{x - x_{\mathrm{sd}}}{x_{\mathrm{ed}} - x_{\mathrm{sd}}}\right)^{n_{\mathrm{d}}} \tag{12}$$

where, x_{sd} is the starting point for wave damping (propagation in the x direction); x_{ed} is the end point for wave damping (boundary); and f_1, f_2, and n_{d} are the parameters of the damping model.

RESULTS

In general, a grid sensitivity study is required before formal calculation to verify the reliability of the grid used. Therefore, the authors conducted a grid sensitivity study before introducing the results of the calculations.

This content downloaded from 159.226.142.168 on Mon, 17 May 2021 09:13:52 UTC
All use subject to https://about.jstor.org/terms

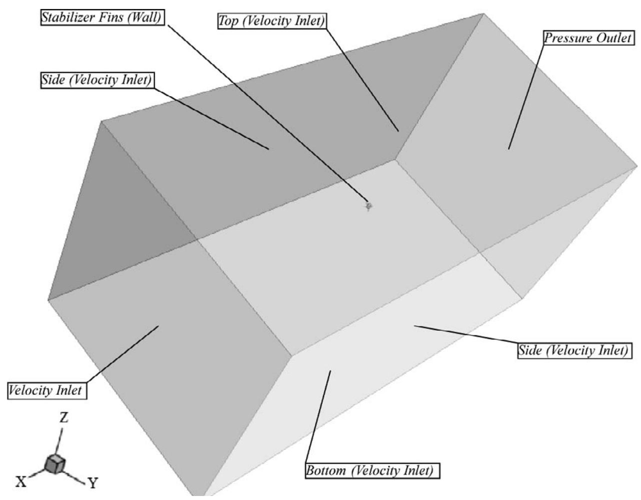

Figure 5. Computational domain.

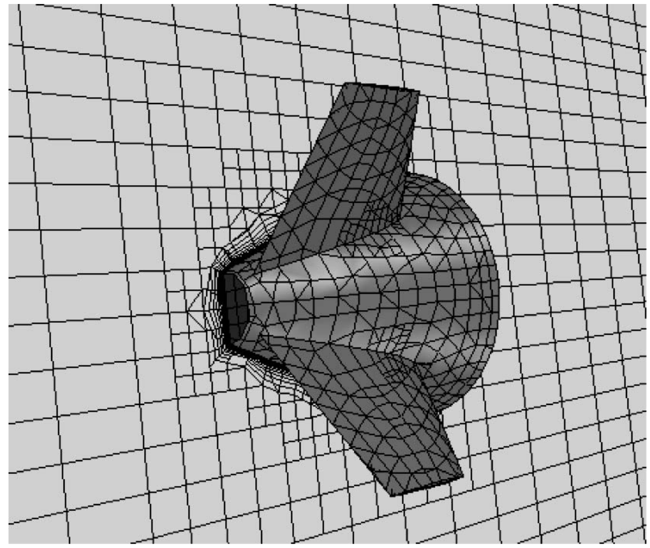

Figure 6. Grids of the submersible's stabilizer fins and cross section.

Mesh Sensitivity Study

The CFD calculations were mainly focused on the buoyancy materials at the stern; the computational domain used in these calculations is shown in Figure 5. The length, width, and depth of the computational domain were 160, 80, and 80 m, respectively. Five trimmed meshes of varying resolutions were generated by STAR-CCM+ for grid-independent validation. The level of the mesh density was changed by adjusting the base size of the grids while keeping the other settings unchanged. The value 0.5 was selected as the 100% base size. A total of 1.3 million grids were generated. The grid of submersible stabilizer fins is shown in Figure 6. The base size of the grids was then changed to 1.13 (226%), 0.935 (187%), 0.635 (127%), and 0.335 (67%) to generate 0.21, 0.32, 0.62, and 2.94 million grids, respectively. A robust automated prism layer meshing algorithm captured the boundary layer, with a two-layer, all $y+$ wall treatment. The $y+$ values were kept in the 30–300 range. The grid settings were based on the grid refinement ratio r_G. In general, the definition of r_G is the ratio of coarse to fine cell sizes, indicating that the refinement factor is simple to compute for a structured grid:

$$r_G = \left(\frac{N_{\text{fine}}}{N_{\text{coarse}}}\right)^{1/d} \tag{13}$$

where, the total number of grids is N, and d is the dimensionality of the computing problem, which in the present study is 3. The grid refinement ratio of fine to medium (medium to coarse) grids in this paper is consistent with (Guo *et al.*, 2017). The maximum of overall moments around the y-axis were calculated under regular waves with an amplitude of 5 m, a wavelength of 40 m, and an inflow angle of 0°. The results are shown in Table 2, indicating that although the five mesh scenarios are under different levels of density, the calculated results for all meshes show little difference. The maximum and minimum values only show 2% difference. Thus, the base size 0.5 was selected for the following calculation.

Calculation Results

In this study, the hydrodynamic analysis of the stabilizer fins were conducted under combinations of one wave condition and three different inflow angles. Figure 7 illustrates the wave inflow angles and the numbering of stabilizer fins. The positive inflow direction is defined as the negative x-axis direction, so an inflow angle of 0° corresponds to a flow toward the stern, and an inflow angle of 180° corresponds to a flow toward the bow. The computations in this study were performed with regular waves of amplitude 5 m and wavelength 40 m. Notice that these conditions correspond to sea state 6 in the Douglas sea scale. The overall profile of the wave is shown in Figure 8. Observed wave conditions of 10 m in front of the stabilizer fins under actual working conditions are shown in Figure 9, and the computed results are shown in Figures 10–12.

ANALYSIS

From the results, it is straight forward to conclude that the wave effects are at the minimum when $a = 180°$ and at the maximum when $a = 90°$. Generally, the stabilizer fins are considerably more affected by the moments in the y-axis than by the moments in the x- or z-axes, because the waves propagate along the x-axis and are uniform along the y-axis. Figures 10b,d and 12b,d indicate that the moments acting on fins 1, 2 and fins 3, 4 are equal in magnitude and opposite in

Table 2. *The maximum of overall moments of different mesh models.*

Mesh No. ($\times 10^6$)	Maximum of Overall Moments around the y-Axis (N m^{-1})
0.21	3.612×10^4
0.32	3.693×10^4
0.62	3.646×10^4
1.30	3.659×10^4
2.94	3.653×10^4

This content downloaded from 159.226.142.168 on Mon, 17 May 2021 09:13:52 UTC
All use subject to https://about.jstor.org/terms

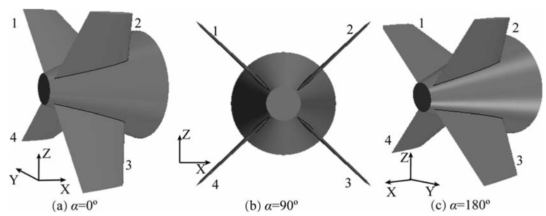

Figure 7. Three different inflow angles used in the calculations.

direction, because the locations of the stabilizer fins are axisymmetric, and their axis of symmetry is aligned with the direction of wave propagation. This arrangement also explains why the moments in the x- and z-axes acting on the stabilizer fins are very small. Additionally, the largest moments acting on the stabilizer fins are observed at fin 3 when $\alpha = 90°$; that is, when the back of the bottom fin is against the inflow, and the maximum moment is 1.7×10^5 N-m. This moment is transferred to the buoyancy materials at the stern, the shapes of which are shown in Figure 13. Theoretically, the buoyancy materials should completely fit on both sides of the structural frame. However, because of inevitable manufacturing flaws and material fatigue from Jiaolong's frequent service in recent years, the structural frame is deformed and the actual contact between the buoyancy materials and the structural frame is limited to region A, as shown in Figure 13. This area is approximately 0.06 m^2, and its distance from the axis is approximately 0.2 m. Therefore, the pressure in this area is approximately 14.2 MPa, which is greater than the shear strength of the buoyancy material (14 MPa).

Although the fins were fixed in the computational model, and the predicted forces could be greater than actual forces, the actual area of contact could be even smaller than the estimated value used in the simulation. Furthermore, only regular waves were used in the numerical model; the actual irregular waves associated with sea state 6 would produce larger moments on the stabilizing fins. The buoyancy materials would suffer serious fatigue from the moments imposed by ocean waves, because they change periodically at relatively high frequency. Therefore, damage quite likely would occur in the contact region between the frame and area A under these conditions, which was also the cause of shear damage in areas B and C. This was the damage mechanism of the buoyancy materials at the bottom of Jiaolong's stern. Additionally, the buoyancy materials on the top of Jiaolong's stern are also subjected to forces that initially increase and then decrease with increasing submergence depth. Damage could occur in the upper buoyancy materials when these forces reach their maximum value.

DISCUSSION

The influence of wave load on the buoyancy materials of the manned submersible was analyzed above and found that the excessive wave load on the manned submersible stabilizer causes shear damage to the buoyant material when the submersible floats on the sea. Here the authors have

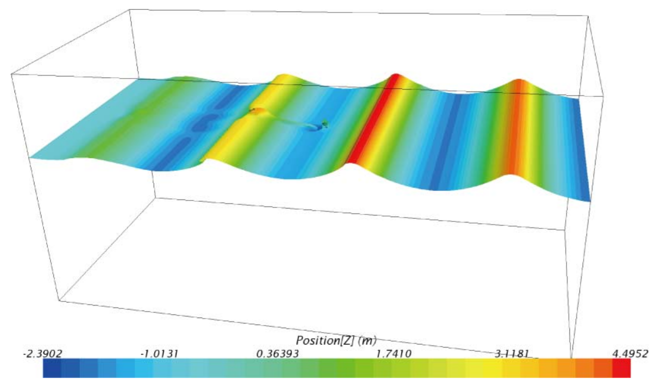

Figure 8. Overall wave profile. (Color for this figure is available in the online version of this paper.)

discussed the effects of deep-sea pressure on the buoyancy materials. The shrinkage of buoyancy materials in water was considered during the design of Jiaolong, as was the loss in buoyancy from shrinkage in this process. However, stress concentrated near the connections of the buoyancy materials from material shrinkage was neglected in Jiaolong's design. According to the bulk modulus of the buoyancy materials, the buoyancy blocks will shrink by approximately 2% at a depth of 7000 m from changes in pressure and temperature. Consider a buoyancy block with an initial length, width, and height of 1 m. At a depth of 7000 m, the volume of the block would reduce to 0.98 m^3 and the length, width, and height of the block would become 0.9933 m, or a decrease of 6.7 mm. Although Jiaolong does not have such a large buoyancy block, it does have blocks whose distance between connection holes is greater than 0.5 m. Therefore, fatal stress (to the submersible) may occur at the connections of these blocks because of underwater shrinkage, which would possibly result in the tension-compression damage or the loosening of pre-embedded parts and is why a considerable amount of tension-compression damage occurred during Jiaolong's 37th Ocean Expedition.

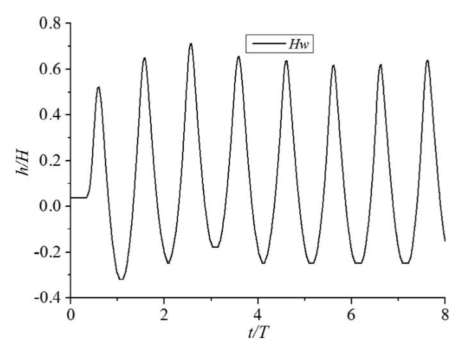

Figure 9. Time series plot of wave heights in front of the stabilizer fin under given waveconditions.

This content downloaded from 159.226.142.168 on Mon, 17 May 2021 09:13:52 UTC
All use subject to https://about.jstor.org/terms

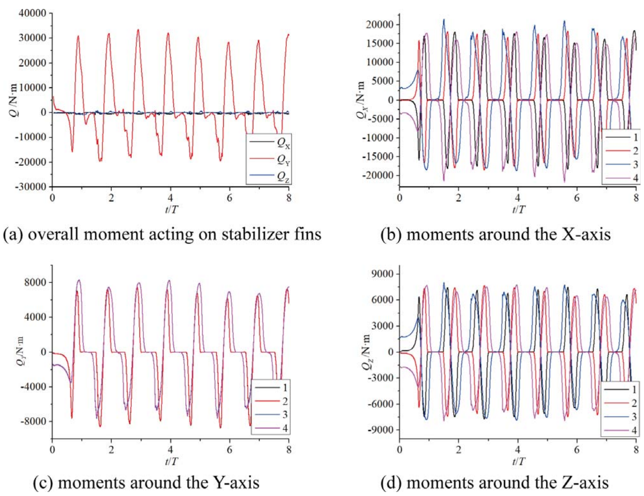

Figure 10. Moments acting on the stabilizer fin at flow angle $\alpha = 0°$. (a) Overall moment acting on the stabilizer fins, (b) moments around the x-axis, (c) moments around the y-axis, (d) moments around the z-axis. (Color for this figure is available in the online version of this paper.)

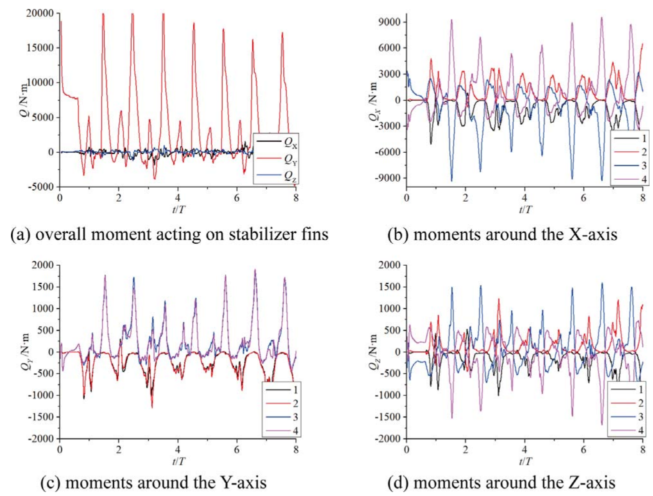

Figure 12. Moments acting on the stabilizer fin at flow angle $\alpha = 180°$. (a) Overall moment acting on the stabilizer fins, (b) moments around the x-axis, (c) moments around the y-axis, (d) moments around the z-axis. (Color for this figure is available in the online version of this paper.)

CONCLUSIONS

The effect of external wave loads on the stern stabilizer fins is at a minimum if the inflow is facing the bow of the submersible and at a maximum if the inflow is facing the sides of the submersible. The shear damage of the buoyancy material is caused by both the excessive moments acting on the stern stabilizer fin and the imperfections of contact between the buoyancy materials and the submersible's structural frame. The reduction of contact area is caused by the deformation of the submersible's structural frame, which occurred during Jiaolong's years of service. Furthermore, the bolts were attached too tightly during installation of the buoyancy blocks, which led to extremely high levels of pressure in certain parts of the submersible. The tension-compression damage and loosening of pre-embedded parts are caused by the shrinkage of the buoyancy materials underwater, which leads to stress concentrated in the connections between the buoyancy materials and the structural frame.

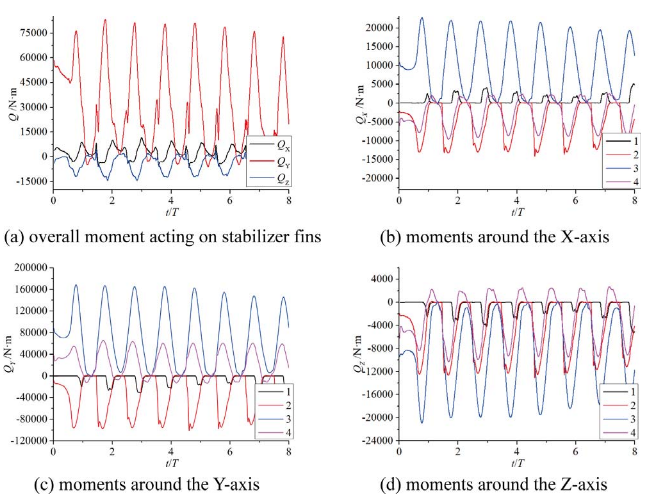

Figure 11. Moments acting on the stabilizer fin at flow angle $\alpha = 90°$. (a) Overall moment acting on the stabilizer fins, (b) moments around the x-axis, (c) moments around the y-axis, (d) moments around the z-axis. (Color for this figure is available in the online version of this paper.)

The following aspects should be considered during the design and usage of deep-sea manned submersibles: They should not be operated in the presence of high waves. The maximum stress of sea state 6 is 14.2 MPa, and the shear strength of buoyant material is 14 MPa. Thus, the operational sea condition must be strictly controlled and kept below sea state 6. If such an extreme sea condition is inevitable, the bow of the submersible should be pointed toward the direction of incoming waves. Long-time operation of the manned submersible on the sea

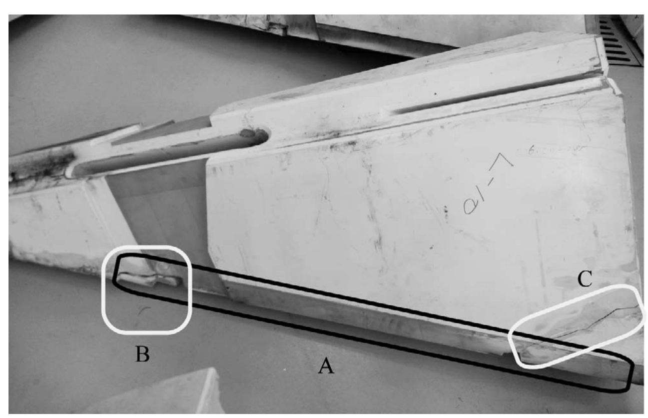

Figure 13. Buoyancy material at the stern.

This content downloaded from 159.226.142.168 on Mon, 17 May 2021 09:13:52 UTC
All use subject to https://about.jstor.org/terms

surface also should be avoided. Additionally, concentrations of stress around connection holes induced by buoyancy material shrinkage should be considered during the design of buoyancy materials used in manned submersibles. For example, embedded parts could be designed with "wiggle room" of 2–4 mm. Moreover, the installation method of the buoyancy blocks should be improved and should be attached by spring washers or ring clamps, which will minimize the effect of stress concentrations on the buoyancy blocks.

ACKNOWLEDGMENTS

This study was supported by the Shandong Province Innovation Talent Plan for Supporting Postdoctoral, Scientific, and Technological Innovation Project of the Qingdao National Laboratory for Marine Science and Technology (2016ASKJ15), the National Key Research and Development Program of China (2017YFC0306600), Taishan Scholars Special Project (TSPD20161007), and the Public Science and Technology Research Funds Projects of the Ocean (201405036).

LITERATURE CITED

Choi, J. and Yoon, S.B., 2009. Numerical simulations using momentum source wave-maker applied to RANS equation model. *Coastal Engineering*, 56(10), 1043–1060.

Cui, W., 2013. Development of the Jiaolong deep manned submersible. *Marine Technology Society Journal*, 47(3), 37–54.

Cui, W.C.; Guo, J., and Pan, B.B., 2018. A preliminary study on the buoyancy materials for the use in full ocean depth manned submersibles. *Journal of Ship Mechanics*, 22(6), 736–757.

Du, Q.; Hu, Y., and Cui, W., 2017. Safety assessment of the acrylic conical frustum viewport structure for a deep-sea manned submersible. *Ships and Offshore Structures*, 12(S1), S221–S229.

Fenton, J.D., 1985. A fifth-order Stokes theory for steady waves. *Journal of Waterway Port Coastal and Ocean Engineering*, 111(2), 216–234.

Gall, M.L.; Choqueuse, D.; Gac, P.Y.L.; Davies, P., and Perreux, D., 2014. Novel mechanical characterization method for deep sea buoyancy material under hydrostatic pressure. *Polymer Testing*, 39, 36–44.

Guo, C.; Wu, T.; Qi, Z.; Luo, W., and Su, Y., 2017. Numerical simulation and experimental studies on aft hull local parameterized non-geosim deformation for correcting scale effects of nominal wake field. *Brodogradnja*, 68(1), 77–96.

Jahsman, W.E., 1968. *Static and Dynamic Material Behavior of Syntactic Foam*. Berlin: Springer Berlin Heidelberg, 387p.

John, B. and Nair, C.P.R., 2010. *Update on Syntactic Foams*. Shawbury, U.K.: Smithers Rapra Technology, 132p.

Johnson, A.A.; Mukherjee, K.; Schlosser, S., and Raask, E., 1970. The behaviour of a cenosphere-resin composite under hydrostatic pressure. *Ocean Engineering*, 2(1), 45–46, IN3–IN4, 47–48.

Kohnen, W., 2013. Review of deep ocean manned submersible activity in 2013. *Marine Technology Society Journal*, 47(5), 56–68.

Li, H.Y.; Zhu, F.F., and Chen, Y.Y., 2016. Preparation and properties of solid buoyancy materials for deep sea with new unsaturated polyesters as matrix. *Key Engineering Materials*, 705, 57–62.

Pasco-Anderson, M. and Watkins, L., 1985. Syntactic foam buoyancy systems for manned & unmanned submersibles. *Proceedings of OCEANS '85—Ocean Engineering and the Environment* (San Diego, California), pp. 1253–1259.

Ren, S.; Hu, X.; Ren, H.; Wang, M.; Guo, A.; Liu, J.; Du, H., and Xian, L. 2017. Development of a buoyancy material of hollow glass microspheres/SiO 2 for high-temperature application. *Journal of Alloys and Compounds*, 721, 213–219.

Stechler, B.G. and Poneros, G.J., 1968. Parametric analysis of optimum buoyancy module designs with computer applications. *Ocean Engineering*, 1(1), 17–37.

Sun, Q.; Wang, Z.P.; Liu, W.; Wang, P., and Wei, H., 2013. Research progress of hollow microsphere composite buoyant material for deep-sea application. *Total Corrosion Control*, 27(9), 31–33.

Walden, B.; Tessier, N., and Popenoe, H., 2010. Newly developed specification and test methods for syntactic foam buoyancy material for deep ocean manned submersible vehicles. *Proceedings of OCEANS 2010 MTS/IEEE SEATTLE* (Seattle, Washington), pp. 1–9.

Zhang, S.Z.; Liang-Min, Y.U.; Chang-Cheng, L.I.; Zhao, H.Z., and Yan-Hong, L.U., 2012. Research development on solid buoyancy material for deep-sea application. *Guangzhou Chemical Industry*, 40(18), 8–10.

Zhang, Z.; Wang, L., and Silberschmidt, V.V., 2017. Damage response of steel plate to underwater explosion: Effect of shaped charge liner. *International Journal of Impact Engineering*, 103, 38–49.

This content downloaded from 159.226.142.168 on Mon, 17 May 2021 09:13:52 UTC
All use subject to https://about.jstor.org/terms